Experimental determination of the neutron resonance peak of ^{162}Er at 67.8 eV

X. X. Li (李鑫祥),[1,2] L. X. Liu (刘龙祥),[1,3,*] W. Jiang (蒋伟),[4,5] J. Ren (任杰),[6] H. W. Wang (王宏伟),[1,3,7,†] G. T. Fan (范功涛),[1,3,7,‡] D. X. Wang (王德鑫),[8] S. Y Zhang (张苏雅拉吐),[8] G. L. Yang (杨高乐),[9] X. K. Li (黎先锴),[2,9] Z. D. An (安振东),[3,9] J. J. He (何建军),[10,11] W. Luo (罗文),[2] X. G. Cao (曹喜光),[1,3,7] L. L. Song (宋龙龙),[1] Y. Zhang (张岳),[4,5] X. R. Hu (胡新荣),[3,7] Z. R. Hao (郝子锐),[3,7] P. Kuang (匡攀),[3,7] B. Jiang (姜炳),[3,7] X. H. Wang (王小鹤),[3] J. F. Hu (胡继峰),[3] Y. D. Liu (刘应都),[12] C. W. Ma (马春旺),[13] Y. T. Wang (王玉廷),[13] J. Su (苏俊),[10,11] L. Y. Zhang (张立勇),[10,11] Y. X. Yang (杨宇萱),[3] S. Feng (冯松),[2] W. B. Liu (刘文博),[3,13] W. Q. Su (苏琬晴),[3,13] S. Jin (金晟),[3,7] and K. J. Chen (陈开杰)[3,14]

[1]*Shanghai Advanced Research Institute, Chinese Academy of Sciences, Shanghai 201210, China*
[2]*School of Nuclear Science and Technology, University of South China, Hengyang 421001, China*
[3]*Shanghai Institute of Applied Physics, Chinese Academy of Sciences, Shanghai 201800, China*
[4]*Institute of High Energy Physics, Chinese Academy of Sciences, Beijing 100049, China*
[5]*China Spallation Neutron Source, Dongguan 523803, China*
[6]*China Institute of Atomic Energy, Beijing 102413, China*
[7]*University of Chinese Academy of Sciences, Beijing 100049, China*
[8]*College of Mathematics and Physics, Inner Mongolia Minzu University, Tongliao 028000, China*
[9]*Sun Yat-sen University, Zhuhai, 510275, China*
[10]*Key Laboratory of Beam Technology and Material Modification of Ministry of Education, College of Nuclear Science and Technology, Beijing Normal University, Beijing 100875, China*
[11]*Beijing Radiation Center, Beijing 100875, China*
[12]*Xiangtan University, Xiangtan 411105, China*
[13]*Henan Normal University, Xinxiang 453007, China*
[14]*ShanghaiTech University, Shanghai 200120, China*

(Received 31 July 2022; revised 17 October 2022; accepted 5 December 2022; published 27 December 2022)

^{162}Er is one of the p nuclei in nuclear astrophysics, and its (n, γ) cross sections are important input parameters in nuclear astrophysics network calculations. Resonance data for ^{162}Er(n, γ) ^{163}Er at 67.8 eV is currently not present in the EXFOR database; however, it is included in the ENDF/B VIII.0 database. The (n, γ) cross section of ^{nat}Er has been measured in the energy range of 1–100 eV at the Back-n facility in the China Spallation Neutron Source. However, due to the influence of the in-beam γ background of the Back-n Facility, it is has not been possible to observe the neutron resonance peak of ^{162}Er at 67.8 eV. A general simulation method is proposed for quantifying the in-beam γ-ray background. By subtracting the in-beam γ-ray background, the neutron-capture yields of ^{162}Er are obtained within the energy range of 20–100 eV. The neutron resonance parameters of ^{162}Er at 67.8 eV are then extracted successfully. It is found that $\Gamma_\gamma = 101.15 \pm 10.08$ meV and $\Gamma_n = 2.79 \pm 0.28$ meV, which are consistent with the ENDF/B VIII.0 database. However, the 51.4-eV resonance peak of ^{162}Er(n, γ) is currently unobserved.

DOI: 10.1103/PhysRevC.106.065804

I. INTRODUCTION

The origin of elements heavier than iron is an important topic in nuclear astrophysics [1]. More than 98% of the heavy elements can be produced by the slow neutron-capture process (s process) [2] and the rapid neutron-capture process (r process) [3]. However, there is still a class of 35 proton-rich nuclides, between ^{74}Se and ^{196}Hg, called p nuclei [4]. They are bypassed by the s and r processes and are typically 10–1000 times less abundant than the corresponding s isotopes and/or r isotopes in the solar system. The common picture is that the p nuclei are synthesized by photodisintegration of pre-existing s- and r-process nuclei via the (γ, n), (γ, p), and (γ, α) reaction channels. ^{162}Er is one of those 35 p nuclei and has a natural abundance of 0.139%. An accurate knowledge of its neutron-capture cross section can help to estimate the (γ, n) reaction rates on the radioactive and short-lived nuclide ^{163}Er.

Although the neutron resonance parameter of ^{162}Er at 67.8 eV is provided by the ENDF/B VIII.0 database [5], it is still unavailable in the newest version of the EXFOR database [6]. Recently, we have performed neutron-capture experiments of erbium [7] at the back-streaming white neutron (Back-n) facility [8,9] of the China spallation neutron source (CSNS) [10–12]. The neutron-capture cross section of erbium was obtained within the 1- to 100-eV energy region. However, it has not been possible to extract the

*Corresponding author: liulongxiang@zjlab.org.cn
†Corresponding author: wanghongwei@zjlab.org.cn
‡Corresponding author: fangongtao@zjlab.org.cn

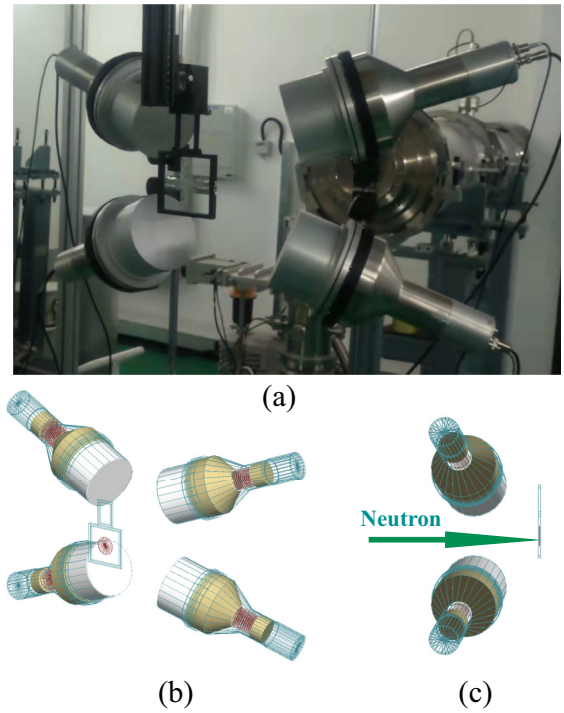

FIG. 1. (a) The photograph of the C_6D_6 detector system. (b) Detector system's construction in simulation. (c) Backward detector layout to minimize background from neutron scattering by the target.

neutron-capture resonance parameters of the ^{162}Er isotope at 67.8 eV due to unavailable data for the in-beam γ-ray background at the Back-n Facility of CSNS.

A general simulation method is proposed for quantifying the in-beam γ-ray background of the Back-n Facility and then the neutron resonance parameters of ^{162}Er at 67.8 eV are extracted successfully for the first time. The time structure measurement and flux simulation for the in-beam γ-ray background are presented. The capture resonance parameters of the ^{162}Er isotope are obtained at 67.8 eV, which is in line with the ENDF/B VIII.0 database.

II. METHOD AND MATERIAL

A. Experiment

The experimental campaigns on neutron-capture cross-section measurement for ^{nat}Er and in-beam γ-ray background detections were carried out at the Back-n Facility of the CSNS, which is mainly used for neutron nuclear data measurements. The energy of neutrons produced at the Back-n Facility ranges from 0.5 eV to 200 MeV and the neutron flux can reach 10^7 cm^{-2} s^{-1}. When the proton accelerator operates in single-bunch mode, the neutron time resolution at 80 m from the spallation target is approximately 0.80% in the energy region of 0.2 eV to 2.8 MeV.

The ^{nat}Er target used for irradiation is 50 mm in diameter and 1 mm in thickness. The uncertainty of target parameters is less than 0.1% (more detailed information is given in Ref. [7]). In order to obtain the (n, γ) cross section for ^{nat}Er, a C_6D_6 (where D denotes ^{2}H) detection system (see Ref. [7]) was used to measure prompt γ rays, which is mainly produced by the neutron-capture reactions on Er isotopes. The C_6D_6 detection system consists of four C_6D_6 scintillation detectors located at the end station 2 (ES2), approximately 76 m away from the spallation target. Each C_6D_6 liquid scintillator is 127 mm in diameter and 76.2 mm in length. The C_6D_6 scintillator is contained in a 1.5-mm-thick aluminum capsule and coupled with a photomultiplier tube (ETEL 9390 KEB PMT) [13]. The layout of the C_6D_6 detector system is shown in Fig. 1. The neutron flux was measured by a Li-Si detector, which is based on the ^{6}Li$(n, \alpha)\,^3$H reaction [14]. Energy spectra are provided by the Back-n Collaboration, and uncertainty is less than 8.0% below $E_n = 0.15$ MeV. The beam power range is from 50 to 52 kW during the experiment. The uncertainty of the beam power is less than 2.0% [7]. The total beam time is over 100 h, and the statistical error is less than 0.2% [7].

In order to determine the in-beam γ-ray shape (time structure), three different Pb targets were used to measure its time structure. Different experimental conditions (target size, filter, and beam power) were used to explore whether the time structure of the in-beam γ background is stable and controllable. In order to exclude the interference of γ rays in the environment, lead targets and empty targets were measured separately in three experiments, and the beam power was 80–100 kW. The details of the three experiments are shown in Table I.

B. Simulation

In-beam γ flux was not measured in the ^{nat}Er neutron-capture experiment. Here we propose a general simulation technique to forecast such in-beam γ-ray flux at a particular energy point of interest. First, we simulate the γ-ray counts recorded by C_6D_6 detectors for a sliver target plus a 40-mm-thick Al filter. Then, in order to confirm that the simulation was valid, we compare the simulated yields with the experimental results [15]. Finally, we update the simulation to

TABLE I. Experimental conditions used for in-beam γ-ray background measurements.

No.	Date	Target	Size	Weight	Duration	Filter	Beam power
1	2020.08	^{nat}Pb	ϕ30 mm × 0.53 mm	4.24 g	7.5 h	With ^{59}Co	80 kW
		Empty	–	–	18 h		
2	2020.10	^{nat}Pb	ϕ40 mm × 0.98 mm	13.92 g	7 h	–	100 kW
		Empty	–	–	9.3 h		
3	2021.04	^{nat}Pb	ϕ30 mm × 0.10 mm	0.79 g	10 h	–	100 kW
		Empty	–	–	10 h		

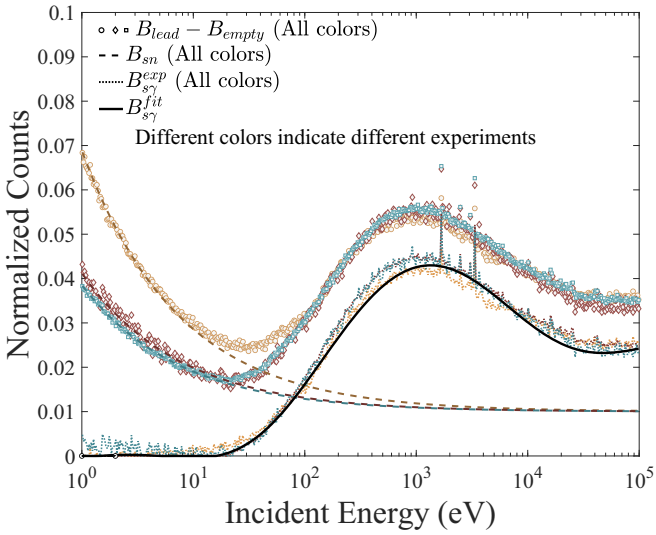

FIG. 2. The time structure of the in-beam γ-ray background. Different line styles represent the experimental and fitted values of different backgrounds, and yellow, blue and red indicate the results of experiments 1–3, respectively. The solid black line indicates the fitted values of $B_{s\gamma}$.

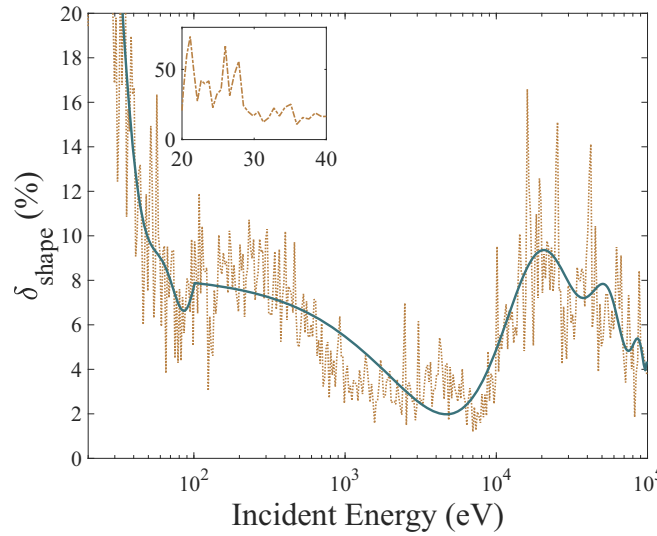

FIG. 3. Shape uncertainties of the in-beam γ-ray background change with time (neutron energy). The maximum occurs at 20 eV with a value of 34.9%.

include a $^{\text{nat}}$Er target in order to calculate the flux of in-beam γ rays for the $^{\text{nat}}$Er experiment.

The detector system was constructed in GEANT4 as shown in Fig. 1. The monoenergy neutron beam with two energies of 34.8 and 86 keV was used to simulate measurement without an ^{27}Al filter. Meanwhile, because the spectrum of in-beam γ rays at different times can be considered unchanged, and the ratio of the flux of the neutrons to the γ ray at the same position is 5.8:1.0 [16], a γ-ray source can be added to the GEANT4 code (the spectrum of neutron and γ rays provided by the Back-n Collaboration, see Refs. [16–18]) to simulate measurement with an ^{27}Al filter.

III. DATA ANALYSIS

A. In-beam γ-ray shape

The background measured by the lead target include the results of neutron and in-beam γ rays scattering from the target:

$$B_{\text{lead}}(E_n) = B_{s\gamma}(E_n) + B_{sn}(E_n) + B_{\text{empty}}(E_n), \qquad (1)$$

where B_{lead} is the result of the lead target; $B_{s\gamma}$ is in-beam γ-ray background; B_{sn} is the neutron-induced background, which exhibits a smooth decrease close to a $1/v$ law [19]; and B_{empty} is the background in the environment under beam conditions, which is determined by measurement of the empty target with the beam. Figure 2 shows the results of $B_{\text{lead}} - B_{\text{empty}}$ under different experimental conditions. The values of $B_{\text{lead}} - B_{\text{empty}}$ can be separated into $B_{s\gamma}$ and B_{sn}. The scatter plots show the experimental results of $B_{\text{lead}} - B_{\text{empty}}$, in which different types of dashed lines indicate the fitted values of B_{sn} and the experimental values of $B_{s\gamma}$ ($B_{\text{lead}} - B_{\text{empty}} - B_{sn}$), respectively. The solid black line indicates the fitted values of $B_{s\gamma}$. Yellow, blue, and red indicate the results of experiments 1–3, respectively.

The experiment 1 is different from others in the total background, which is due to the placement of the ^{59}Co filter at the beamline. The atomic number of ^{59}Co is 27 and the thickness is only 0.4 mm, its influence on the beam is limited to the neutron part, and the impact on γ rays is small. Under different experimental conditions, the experimental values of separated $B_{s\gamma}(E_n)$ are similar and can be fitted with the same curve. The form of the curve can be expressed by

$$B_{s\gamma}^{\text{fit}}(E_n) = \begin{cases} 0 & (E_n \leqslant 2\times10^{-5}\,\text{MeV}), \\ f(E_n) & (E_n > 2\times10^{-5}\,\text{MeV}), \end{cases} \qquad (2)$$

where E_n is the neutron energy in MeV. In the energy region $E_n \leqslant 20$ eV, there is no substantial influence of in-beam γ rays, whereas in the energy region of $E_n > 20$ eV, the time structure of the in-beam γ rays is determined by the following [15,19,20]:

$$f(E_n) = \frac{a_1}{\sqrt{E_n}} + a_2 e^{a_3/\sqrt{E_n}} + a_4 e^{a_5\sqrt{E_n}} + a_6, \qquad (3)$$

where a_i are the fitting parameters, and $a_1 = -5.343e-6$, $a_2 = 0.146$, $a_3 = -0.016$, $a_4 = 0.122$, $a_5 = -17.7$, and $a_6 = -0.115$. These parameters can narrow the gap between $B_{s\gamma}^{\text{fit}}$ and the averaged $B_{s\gamma}^{\text{exp}}$. The neutron-capture cross section of $^{\text{nat}}$Pb has obvious resonance peaks at $E_n = 1.6$ keV and $E_n = 3.3$ keV. The resulting values of $B_{s\gamma}^{\text{exp}}$ are significantly higher than the fitted ones. In our case, $B_{s\gamma}^{\text{fit}}$ is more reliable than $B_{s\gamma}^{\text{exp}}$ because it excludes the contribution of the γ rays generated by the neutron-capture reaction of the natural lead target. It suggests that the ^{208}Pb isotope target is better than the natural one for in-beam γ-ray measurement because it has fewer neutron-capture resonance peaks between 1 eV and 100 keV.

The deviation of $B_{s\gamma}^{\text{fit}}$ from the averaged $B_{s\gamma}^{\text{exp}}$, δ_{shape}, is obtained. The result is presented in Fig. 3. When the neutron energy is greater than 100 eV, the deviation values are less than 8%. The deviation curve exhibits a clear oscillation as a result of the $^{\text{nat}}$Pb's neutron-capture reactions. As seen in

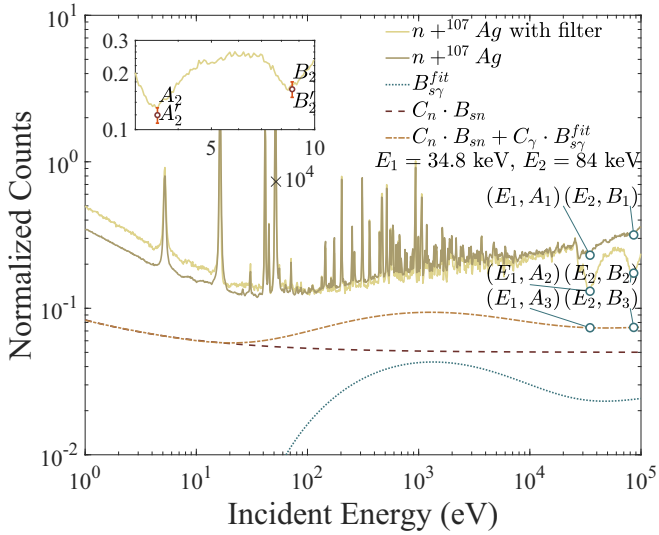

FIG. 4. Experimental spectra for Ag target with and without the Al filter, together with $B_{s\gamma}^{\rm fit}$, C_nB_{sn}, and $C_nB_{sn}+C_\gamma B_{s\gamma}^{\rm fit}$. Here C_n and C_γ are the coefficients of the neutron and γ-ray scattering backgrounds, respectively. The value of C_n can be obtained from Ref. [7] and the determination of C_γ is discussed later. The inset shows the enlarged spectrum for the Ag target plus the Al filter, which is in the energy range between 30 and 100 keV. Red dots with error bars represent the simulated counting spectrum at the two ^{27}Al absorption peaks mentioned above.

Fig. 3, the aforementioned volatility can be smoothed down by fitting a fourth-order Fourier series.

B. In-beam γ-ray flux

Figure 4 shows the solid lines indicate the counting spectrum for the Ag target (normalized by the neutron flux rate) with and without the Al filter, and the dashed lines show the fitting curves of $B_{s\gamma}$ and B_{sn}. A_1 and B_1 are the counting spectrum at $E_n = 34.8$ keV and $E_n = 86$ keV for the Ag target experiment without an Al filter, while A_2 and B_2 are the counting spectrum for the Ag target experiment with an Al filter. Accordingly, A_1', A_2', B_1', and B_2' are the simulated values. The simulated yields at the Al absorption peaks of $E_n = 34.8$ keV and $E_n = 86$ keV are in good agreement with the experimental ones, indicating the simulation is able to predict the counting spectrum. More simulation details are presented in Sec. II B.

Generally, the ratio(s) between the values of A_1 (A_1') and A_2 (A_2') are constant, i.e.,

$$A_1/A_2 = C_1,$$

$$A_1'/A_2' = C_2. \tag{4}$$

For the Ag target at $E_n = 34.8$ keV, we define the coefficient C as C_2/C_1, which represents the variation between the experimental and simulated values. The value of B_2 can then be calculated based on the values of B_1, B_1', and B_2'. It shows good agreement between the simulated and experimental values within the bounds of statistical uncertainty. In our case, the coefficient C is equal to 1, demonstrating its independence from both the incident energy and the target. As a result, the value of A_2 for the $^{\rm nat}$Er target with the Al filter at $E_n = 34.8$ keV can be obtained with

$$A_{2,\rm Er} = CA'_{2,\rm Er}\frac{A_{1,\rm Er}}{A'_{1,\rm Er}}. \tag{5}$$

Here, $A_{1,\rm Er}$ is the counting spectrum obtained in the $^{\rm nat}$Er target experiment without the Al filter, and $A'_{1,\rm Er}$ and $A'_{2,\rm Er}$ are the simulated values without and with the Al filter, respectively.

It is still possible for neutrons with energy at the peak of ^{27}Al absorption to escape the Al filter and reach the target; according to simulations, the uncertainty is expected to be less than 6%. The widths of the two ^{27}Al absorption peaks can also result in an uncertainty of 5% for determination of the neutron flux at these energies. In addition, the value of C may not be exactly the same for different absorption peaks. The resulting uncertainty is ceil{max(C_i)%} and its value is approximated to be 5%. Here ceil is the round up function and C_i is the ith absorption peaks. As a result, in our case the scaled uncertainty is $\delta_{\rm scale} \approx 9.3\%$.

C. Neutron capture yield

The in-beam γ background for the $^{\rm nat}$Er experiment can be expressed as

$$B^{\gamma}_{\text{in-beam}}(E_n) = C_\gamma B_{s\gamma}(E_n), \tag{6}$$

where C_γ is the scale parameter of the in-beam γ-ray flux and $B_{s\gamma}(E_n)$ is the in-beam γ-ray shape. As shown in Fig. 4, A_3 and B_3 are the values of $C_nB_{sn}+C_\gamma B_{s\gamma}^{\rm fit}$ at $E_n = 34.8$ and 86 keV, respectively. Let $A_3 = A_2\sigma_1/\sigma_2$ and $B_3 = B_2\sigma_1/\sigma_2$, where σ_1 and σ_2 are the γ-ray scattering cross sections of lead and $^{\rm nat}$Er targets at $E_n = 34.8$ and 86 keV, respectively. GEANT4 simulations can be used to determine the values of σ_1 and σ_2 because the energy spectra of in-beam γ rays do not change with E_n [16]. The value of C_γ can then be obtained.

The pulse height weighting technique has been widely used in neutron-capture cross-section measurements with C_6D_6 detector [21,22]. Combining an accurate weighting function

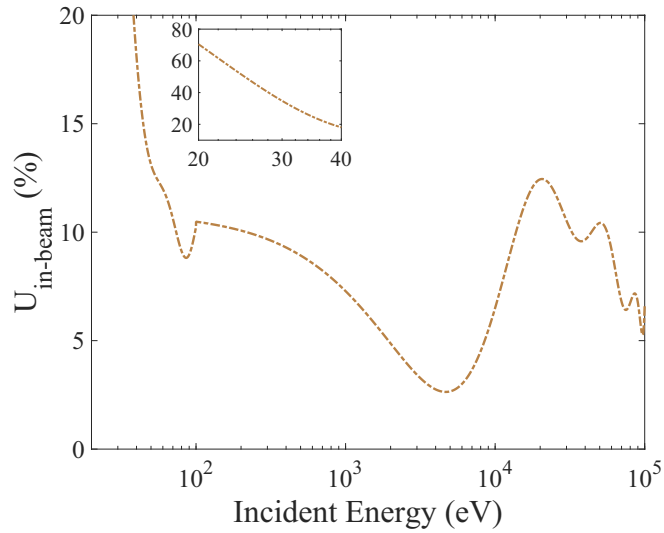

FIG. 5. The uncertainty of δ_{Y_w} as a function of E_n.

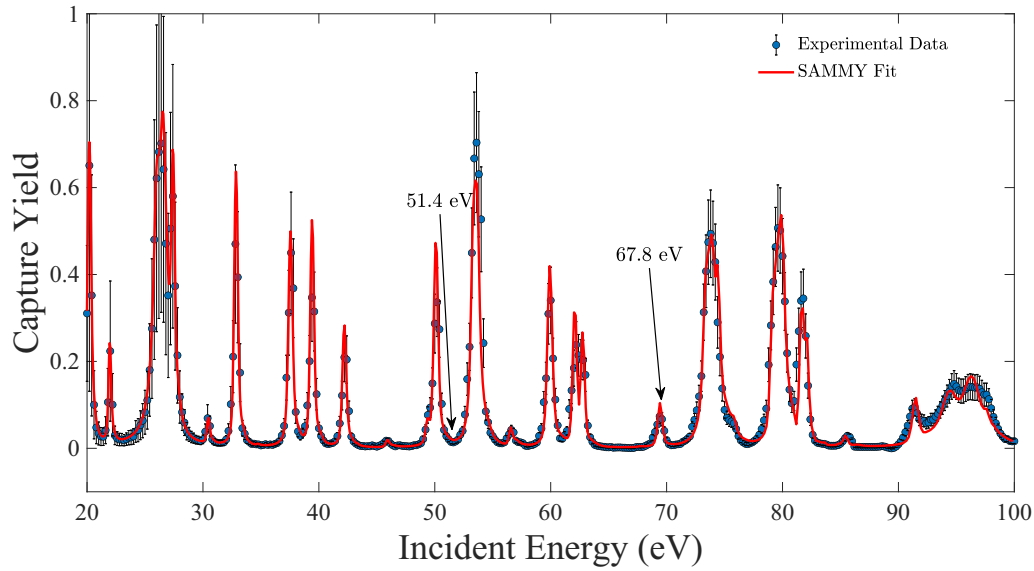

FIG. 6. The experimental capture yields and the fitted ones obtained with the SAMMY code.

(WF), such a technique enables the detection efficiency to be independent of the cascaded γ-ray energy. The WF of $^{\text{nat}}$Er can be found in Ref. [7]. Its uncertainty is less than 3.0%.

In this study, the WF of $^{\text{nat}}$Er is applied to obtain the weighted spectrum $N_w(E_n)$ by weighting the net spectrum $N(E_n)$. $N(E_n)$ is obtained by subtracting the in-beam γ-ray background from $N_{\text{past}}(E_n)$ and can be written as

$$N(E_n) = N_{\text{past}}(E_n) - B^{\gamma}_{\text{in-beam}}(E_n). \tag{7}$$

Here $N_{\text{past}}(E_n) = N_{\text{Er,past}} - B_{sn,\text{past}} - B_{\text{empty,past}}$. Note that $N_{\text{Er,past}}$, $B_{sn,\text{past}}$, and $B_{\text{empty,past}}$ have been obtained in the previous $^{\text{nat}}$Er experiment [7] and $N_{\text{Er,past}}$ is the normalized counting spectrum. The capture yield is dependent on $N_w(E_n)$ and its expression can be written as

$$Y_w(E_n) = \frac{N_w(E_n)}{N_s I(E_n) S_n}, \tag{8}$$

where N_s is the areal number density of the target nuclides, $I(E_n)$ is the neutron flux provided by the Back-n Collaboration [18], and S_n is the neutron binding energy. For the $^{\text{nat}}$Er targets, their isotopes contribute to a set of resonance peaks at different energies. The values of S_n for $^{\text{nat}}$Er isotopes can be obtained according to the NuDat-2.0 database [23].

According to Eq. (8), the uncertainty of the neutron-capture yield mainly originates from the $^{\text{nat}}$Er neutron-capture measurement and the in-beam γ-ray background. The measurement uncertainty is caused by experimental conditions, data analysis, and statistical uncertainty. The value is less than 8.8% [7]. The uncertainty of the in-beam γ-ray background ($B^{\gamma}_{\text{in-beam}} = C_{\gamma} B_{s\gamma}$) can be obtained with

$$\delta^2_{\text{in-beam}} = \left(\frac{\partial B}{\partial B_{s\gamma}}\right)^2 \delta^2_{\text{shape}} + \left(\frac{\partial B}{\partial C_{\gamma}}\right)^2 \delta^2_{\text{scale}}. \tag{9}$$

The uncertainty of the capture yield (δ_{Y_w}), as determined by the uncertainty propagation formula, is displayed in Fig. 5. δ_{Y_w} can be divided into three energy areas: (a) $E_n < 218$ eV, (b) $E_n \in [218\text{ eV}, 13.8\text{ keV}]$, and (c) $E_n > 13.8$ keV. In region (a), the values of δ_{Y_w} can be greater than 15% because of the significant shape uncertainty, particularly when $E_n < 40$ eV. In region (b), thanks to the success of in-beam γ-ray shape fitting, the value of δ_{Y_w} is under 15%. In region (c), the increased neutron-capture cross section of the natural lead target causes a noticeable fluctuation in the δ_{Y_w}.

TABLE II. Resonance parameters were extracted from the R-matrix analysis and compared to those in the ENDF/B-VIII.0 evaluation database.

			ENDF/B-VIII.0			Previous work [7]			This work		
Mass	J	g	E_R (eV)	Γ_γ (meV)	Γ_n (meV)	E_R (eV)	Γ_γ (meV)	Γ_n (meV)	E_R (eV)	Γ_γ (meV)	Γ_n (meV)
162	0.5	1.0	20.3	100.0	8.3	20.2	100.4 ± 9.8	8.3 ± 0.6	20.2	100.6 ± 10.1	8.2 ± 0.9
			34.8	100.0	5.1	34.8	105.19 ± 10.1	3.1 ± 0.3	34.7	108.3 ± 10.6	4.7 ± 0.5
			43.2	100.0	2.2	44.5	101.47 ± 8.3	2.1 ± 0.1	43.3	99.9 ± 10.0	2.1 ± 0.2
			46.0	100.0	19.5	45.9	117.66 ± 10.1	16.9 ± 1.5	45.9	115.2 ± 13.3	18.9 ± 1.4
			51.4	100.0	52.0	–	–	–	–	–	–
			57.0	100.0	32.0	56.6	101.50 ± 9.9	13.0 ± 1.3	56.8	102.5 ± 11.0	32.0 ± 1.5
			67.8	100.0	3.1	–	–	–	67.7	101.2 ± 10.1	2.8 ± 0.3

IV. RESULTS AND DISCUSSION

According to Eq. (8), we subtract the $B^{\gamma}_{\text{in-beam}}(E_n)$ from the $N_{\text{past}}(E_n)$ and then obtain the Y_w for the $^{\text{nat}}\text{Er}(n,\gamma)$ reactions (see Fig. 6). The data of Y_w was fitted by the *R*-matrix code SAMMY [24], considering various experimental effects such as Doppler broadening [25], self-shielding, and multiple scattering. The resonance parameters of $^{\text{nat}}\text{Er}(n,\gamma)$ are then extracted accordingly. The fitting result is also shown in Fig. 6. A resonance peak of $^{162}\text{Er}(n,\gamma)$ at 67.8 eV is found successfully, and the resonance parameters are $\Gamma_\gamma = 101.15 \pm 10.08$ meV and $\Gamma_n = 2.79 \pm 0.28$ meV. However, it does not occur in our previous data analysis due to the interference of in-beam γ-ray background [7]. Benefiting from the general simulation method for quantifying $B^{\gamma}_{\text{in-beam}}(E_n)$, such a resonance peak is observed experimentally for the first time.

The resonance peak of the $^{\text{nat}}\text{Er}(n,\gamma)$ at 51.4 eV is predicted by ENDF/B VIII.0 database and the production cross section is as large as ≈5600 b. However, this resonance peak does not occur in the subtracted Y_w, as shown in Fig. 6. Meanwhile, other resonance peaks with lower production cross sections have been found within the energy range of 20–100 eV, such as the resonance peaks at 34.8 eV (≈1300 b), 43.20 eV (≈500 b), and 67.8 eV (≈200 b). We call for additional experiments to confirm the existence of this resonance.

At resonance energies of 34.8, 46, and 57 eV, as depicted in Fig. 6, the yields of $^{\text{nat}}$Er's neutron capture are quite modest. Table II displays a comparison between the ENDF/B-VIII.0 database and the currently available experimental data. As shown in Fig. 7, the values of Γ_n in the present work are closer to those offered by the ENDF/B-VIII.0 database than previous data. It suggests that the $^{162}\text{Er}(n,\gamma)$ resonance parameters provided by this work are more reliable than those offered by previous study because the significant in-beam γ-ray background can be removed using the proposed general method.

V. SUMMARY AND CONCLUSIONS

The in-beam γ-ray background is crucial for neutron-capture cross-section experiments at the Back-n Facility. In this work, we have presented a general method to subtract the in-beam γ-ray background of the $^{\text{nat}}\text{Er}(n,\gamma)$ experiment. The time structure and the flux of the in-beam γ-ray background are obtained through experiment and GEANT4 simulation, respectively. This general method is then applied successfully to calculate the neutron-capture yield. The neutron-capture resonance parameters of ^{162}Er at 67.8 eV are extracted for the first time. It is found that the resonance parameters are $\Gamma_\gamma = 101.15 \pm 10.08$ meV and $\Gamma_n = 2.79 \pm 0.28$ meV. Our results are consistent with the ENDF/B VIII.0 database within the uncertainty range.

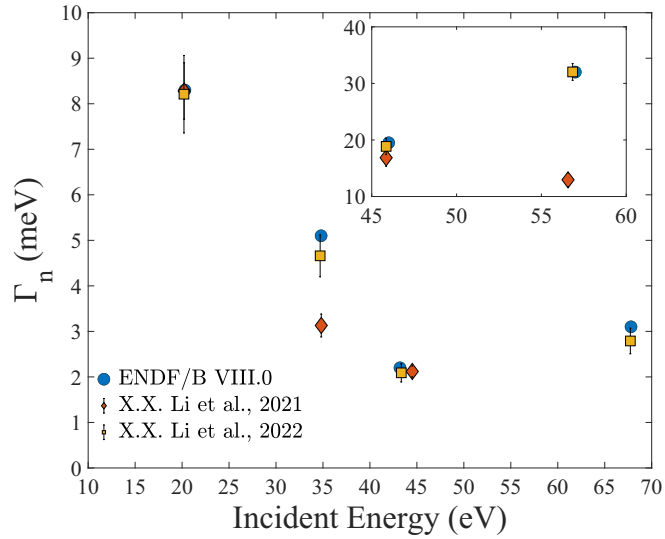

FIG. 7. Comparison between the Γ_n values obtained from the ENDF/B-VIII.0 database, previous data [7], and this work. The inset shows a range of 10 to 40 meV for the *y* axis.

Our general method is still valid for in-beam γ-ray background analysis when the incident energy is higher than 100 eV. Currently, due to the lack of sufficient in-beam γ-ray background data at the Back-n Facility, it is hard to accurately obtain neutron-capture resonance parameters in such energy region for a set of targets including the ^{197}Au target [26], the $^{\text{nat}}$Lu target [20], ^{232}Th target [28] and the $^{\text{nat}}$Se target [27]. In order to get more beneficial experimental nuclear data for nuclear astrophysics, we then expect quantifying the in-beam γ-ray background in a relative high-energy region will be needed.

ACKNOWLEDGMENTS

We appreciate effective technical support from Dr. Yi-Jie Wang at Tsinghua University, Dr. Yu-Chao Xu at General Electric, Dr. Xing-Yuan Xu at University of Science and Technology of China, Xin-Yu Li at ChongQing University, and the efforts of the staff of the CSNS and Back-N Collaboration. This work was supported by the National Natural Science Foundation of China under Grants No. 11875311, No. 11905274, No. 1705156, No. U2032146, No. 11865010, No. 11765015, and No. 1160509; the Natural Science Foundation of Inner Mongolia under Grants No. 2019JQ01 and No. 2018MS01009; and the Strategic Priority Research Program of the CAS (Grant No. XDB34030000).

[1] R. Reifarth, C. Lederer, and F. Käppeler, J. Phys. G: Nucl. Part. Phys. **41**, 053101 (2014).
[2] F. Käppeler, R. Gallino, S. Bisterzo *et al.*, Rev. Mod. Phys. **83**, 157 (2011).
[3] J. J. Cowan, F. K. Thielemann, and J. W. Truran, Phys. Rep. **208**, 267 (1991).
[4] M. Arnould and S. Goriely, Phys. Rep. **384**, 1 (2003).
[5] D. A. Brown, M. B. Chadwick, R. Capote *et al.*, Nucl. Data Sheets **148**, 1 (2018).
[6] V. V. Zerkin and B. Pritychenko, Nucl. Instrum. Methods Phys. Res., Sect. A **888**, 31 (2018).

[7] X. X. Li, L. X. Liu, W. Jiang *et al.*, Phys. Rev. C **104**, 054302 (2021).
[8] J. Y. Tang, Q. An, J. B. Bai *et al.*, Nucl. Sci. Tech. **32**, 11 (2021).
[9] Z. Q. Cui, H. Y. Jiang, W. Jiang *et al.* (CSNS Back-N Collaboration), Eur. Phys. J. A **57**, 310 (2021).
[10] H. Chen and X. L. Wang, Nat. Mater. **15**, 689 (2016).
[11] J. B. Yu, J. X. Chen, L. Kang *et al.*, Nucl. Sci. Tech. **28**, 46 (2017).
[12] X. M. Jin, Y. Liu, C. L. Su *et al.*, Nucl. Sci. Tech. **30**, 143 (2019).
[13] J. Ren, X. C. Ruan, J. Bao *et al.*, Radiat. Detect. Technol. Methods **3**, 52 (2019).
[14] Q. Li, G. Y. Luan, J. Bao *et al.*, Nucl. Instrum. Methods Phys. Res. A **946**, 162497 (2019).
[15] X. X. Li, L. X. Liu, W. Jiang *et al.*, Chin. Phys. B **31**, 038204 (2022).
[16] J. Ren, X. C. Ruan, Y. H. Chen *et al.*, Acta Phys. Sin. **69**, 172901 (2020).
[17] J. Ren, X. C. Ruan, W. Jiang *et al.*, Nucl. Instrum. Methods Phys. Res., Sect. A **985**, 164703 (2021).
[18] Y. H. Chen, G. Y. Luan, J. Bao *et al.*, Eur. Phys. J. A **55**, 115 (2019).
[19] C. Lederer, N. Colonna, C. Domingo-Pardo *et al.* (n_TOF Collaboration), Phys. Rev. C **83**, 034608 (2011).
[20] D. X. Wang, S. Y. L. T. Zhang, W. Jiang *et al.*, Acta Phys. Sin. **71**, 072901 (2022).
[21] R. L. Macklin and J. H. Gibbons, Phys. Rev. **159**, 1007 (1967).
[22] U. Abbondanno, G. Aerts, H. Alvarez *et al.*, Nucl. Instrum. Methods Phys. Res., Sect. A **521**, 454 (2004).
[23] A. A. Sonzogni, AIP Conf. Proc. **769**, 574 (2005).
[24] N. M. Larson, Updated users' guide for sammy multilevel R-matrix fits to neutron data using bayes' equation[R]. Oak Ridge National Lab.(ORNL), Oak Ridge, TN (United States), 1998.
[25] B. Jiang, J. L. Han, W. Jiang *et al.*, Nucl. Instrum. Methods Phys. Res., Sect. A **1013**, 165677 (2021).
[26] X. R. Hu, L. X. Liu, W. Jiang *et al.*, Nucl. Sci. Tech. **32**, 101 (2021).
[27] X. R. Hu, L. X. Liu, W. Jiang *et al.*, Chin. Phys. B **31**, 080101 (2022).
[28] B. Jiang, J. L. Han, J. Ren *et al.*, Chin. Phys. B **31**, 060101 (2022).